Analytical and Computational Models of Rijke Tube Pressure Waveforms Using a Sigmoidal Temperature Distribution

Emma T. Signor* and Joseph Majdalani†
Auburn University, Auburn, AL 36849

In this work, an asymptotic expansion technique is paired with a naturally occurring small perturbation parameter within the framework of a one-dimensional tube featuring an open-open endpoint configuration and a spatially variable heat source. Integrating the resulting equations with a spectral collocation eigensolver, accurate predictions of acoustic pressure mode shapes and frequencies are achieved across a broad parametric spectrum. Our analysis encompasses variations in the temperature gain across the heat source, the heat source length and position, and the overall thermal profile, in a manner to emulate diverse flow heating configurations that are characteristic of Rijke tubes. In this work, we focus on a globally applied sigmoidal temperature distribution, which leads to a uniformly valid, continuous, and differentiable thermal profile spanning the entire tube, including the rapid variations across the heat source element. Our mathematical procedure relies on Green's functions and an integral formulation that enables us to extract all acoustic frequencies analytically in closed form. These frequencies are found to exhibit a monotonic increase with successive increments in temperature gains, reductions in heat source lengths, retraction of the heat source, and smoothing of the temperature gain across the heat source. Similarly, pressure mode shapes are found to display blunter and often linear variations for higher temperature gains, longer heat sources, and downward displacements of the heat source towards the inlet.

Nomenclature

a_0	mean speed of sound inside the Rijke tube
${}_2F_1$	confluent hypergeometric function
f	Hertzian frequency
f_p	initial pressure
G_p	Green's function
g_p	initial pressure derivative
L	Rijke tube length
l_c	combustor flame zone length
n	oscillation mode number
p'	oscillatory pressure component
q'_ϑ	unsteady heat release per unit volume
R	specific gas constant
T	temperature
t	time
u'	oscillatory velocity component
x	axial distance from the inlet
x_f	flame zone leading edge measured from the inlet
x_s	midpoint of the sigmoidal profile measured from the inlet

Greek

α	normalized temperature gain at aft end, $(T_0)_{\max}/(T_0)_{\min}$
β	sigmoidal curve steepness or growth rate
γ	average ratio of specific heats
ϵ	perturbation parameter, $(\gamma-1)/\gamma$
Θ	temperature-based integral, $n\pi/\tilde{\omega}_n$
ρ	air density
ω	circular frequency

*Undergraduate Research Assistant, Department of Aerospace Engineering, Student Member AIAA.
†Professor and Francis Chair, Department of Aerospace Engineering, Fellow AIAA.

Subscripts and Superscripts

c	combustor or heat source property
f	flame zone property
n	oscillation mode number, $n = 1, 2, ...$
0	steady or mean component
$\tilde{}$	normalized quantity

I. Introduction

COMBUSTION devices, particularly those incorporating spatially distributed heat sources, have been the subject of dedicated research investigations aimed at understanding the fundamental mechanisms affecting their performance and stability. These factors are particularly relevant to rockets and thermoacoustic devices, such as Rijke and Soundhauss tubes, which have attracted considerable attention in the propulsion community. In this context, several studies have been pursued with the objective of gaining a deeper physical understanding of the thermoacoustic phenomena and criteria that prescribe the optimal functionality of these combustors. Among them, the reader may be referred to the technical articles by Carrier [1], Chu [2], Miller and Carvalho [3], Maling [4], Zinn [5], as well as a survey by Raun et al. [6].

Despite these complementary efforts, one aspect of Rijke tube operation that continues to escape our understanding is the detailed interaction between the thermal pattern generated by the heat source and the resulting acoustic waveform. While several theoretical models have been proposed to explore the nonlinear relations between the heat source and acoustic pressure oscillations, their ability to predict the complex thermoacoustic interactions observed in experiments has been somewhat limited to specific, user-defined conditions. These include sudden temperature jumps, simple thermal patterns, or idealistic boundary conditions [7–9].

In the context of a Rijke tube, specifically, the coupling between unsteady heat and acoustic disturbances extends over two distinct regions. These remain separated by a diffuse region often modeled as a zonal discontinuity at the heat source location. The accurate modeling of the temperature profile across this discontinuity and throughout the tube has been shown to strongly influence the accuracy of the ensuing pressure and velocity oscillations [10–12]. Consequently, understanding the complexities of unsteady flow-heat transfer interactions across different segments of a Rijke tube continues to be a focal point in the thermoacoustic and propulsion communities.

It may be worth noting that in the development of industrial, propulsive, and power generation devices, the establishment of favorable thermoacoustic conditions is not merely advantageous, but rather essential. Achieving and maintaining proper thermoacoustic conditions, which is often realized through iterative "cut and try" methods, has been crucial in reducing operational costs. It has also proven beneficial at enhancing combustion efficiency, suppressing instability, promoting fuel savings, reducing pollutant formation, and increasing convective heat transfer rates [13–17]. These improvements have been closely linked to the judicious control of the evolving acoustic field, which directly impacts the overall performance of various combustors. Depending on the application at hand, the main objective can be to either promote or suppress thermoacoustic coupling. On the one hand, maintaining so-called "resonant states" can be beneficial for thermal efficiency, flame holding, mixing enhancement, and heating or cooling. On the other hand, undesired thermoacoustic triggering can lead to excessive vibrations, noise, and thermal stresses, and these do not only compromise motor performance and structural integrity, but also lead to outright system failure in rocket systems [18, 19].

Bearing these miscellaneous factors in mind, the present work aims at furthering our understanding of heat-driven pressure oscillations in a Rijke tube. Building on previous research efforts that focus on analyzing the thermoacoustic field in an open-open Rijke tube configuration [20], this study follows a three-pronged approach that combines theoretical, experimental, and numerical analyses in the process of predicting the acoustic pressure mode shapes and frequencies in an open-ended enclosure. The resulting approach, which imposes a user-specified temperature distribution upstream and downstream of the heat source, will be used to model the induced thermoacoustic field. At the outset, a closed-form analytical formulation will be obtained and used to supplement a computationally generated eigensolution for the pressure oscillations and frequencies evolving in a simulated Rijke tube.

To proceed, the work will closely examine the effect of implementing a realistic sigmoidal temperature profile that is capable of capturing the rapid thermal jump across the heat source while seamlessly extending uniformly over the entire length of the tube. This investigation constitutes an essential sequel to prior work that devoted itself primarily to

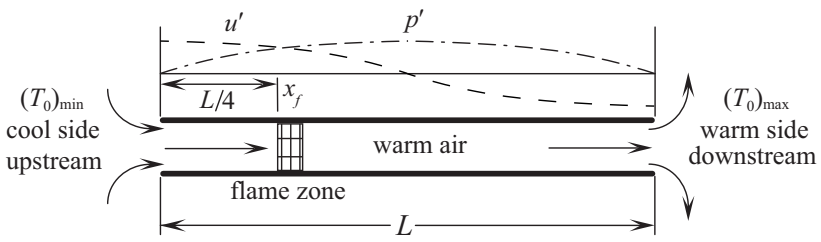

Fig. 1. Rijke tube of length L and combustor flame zone thickness l_c that is placed at an initial axial station of $x_f = L/4$. For convenience, this vertical tube is oriented horizontally and modeled as a case of one-dimensional, inviscid, and adiabatic motion with constant thermophysical properties.

the adaptation of different temperature profiles before and after the heat source [20].

From an organizational standpoint, this article is structured as follows. Section II briefly outlines the basic assumptions and equations governing the use of a variable temperature gradient and an unsteady heat release. Our approach builds upon an integral formulation derived asymptotically by Shelton and Majdalani [20] for pressure eigenfrequencies and eigensolutions. This formulation is based on a leading-order perturbation approximation that is solvable using Green's functions. While a closed-form asymptotic solution for the pressure waveform is provided for arbitrary temperature distributions, we rely on a robust spectral collocation eigensolver to evaluate and describe the resulting mode shape patterns under steep temperature gradients.

In Section III, we analyze the impact of a finite temperature zone on pressure oscillations using a sigmoidal pattern that can be globally adjusted to mimic realistic thermal patterns throughout the tube. This profile is chosen because of its suitability to emulate empirical temperature distributions that have been reported in thermoacoustic devices. To this end, we evaluate multiple thermal configurations that allow for variations in the final temperature downstream of the flame zone, as well as the initial location and length of the flame zone or heat source element.

Section IV investigates the connection between the frequency and the thermal characteristics of the sigmoidal distribution. In this process, the defining frequency integral is evaluated analytically in a manner to explicitly reproduce the eigenmodes associated with the sigmoidal profile. All asymptotic results are verified numerically through comparisons to other open-source eigensolvers, such as those by Ledoux and Van Daele [21].

II. Problem Formulation

A. Fundamental Assumptions and Dimensionless Variables

In the context of the Rijke tube geometry detailed in Fig. 1, one can simplify the system as a one-dimensional, inviscid, and adiabatic motion with constant thermophysical properties, assuming no mean heat input or velocity. Here, x_f represents the initial axial location of the combustor flame zone, which extends over a total length of l_c. We treat the air as a perfect gas with constant mean pressure and a temperature distribution that varies only with the axial coordinate. While thermoacoustic instabilities typically involve three disturbance modes [22], we focus only on the acoustic and entropic modes, disregarding the vortical mode. This is justified by virtue of our inviscid and one-dimensional spatial assumptions. Under these auspices, we can relate the density to the pressure and specific entropy s. Thereupon, by using the subscript "0" for mean values and a prime for fluctuating, time-dependent disturbances, all instantaneous variables may be decomposed into mean and unsteady quantities, assuming a negligible mean flow velocity. This decomposition may be realized using $p = p_0 + p'$, $\rho = \rho_0 + \rho'$, and $u = u'$. Here, $R = p_0/(\rho_0 T_0)$ represents the specific gas constant for an ideal gas, and $\gamma = C_p/C_v$ stands for the ratio of specific heats. Additionally, we define q'_ϑ to be the fluctuating heat release rate per unit volume. This decomposition enables us to linearize the mass and momentum equations [23]. Following the terminology introduced in Ref. [20], all spatial and temporal variables may be normalized. Thus, using a_0 for the average speed of sound within the Rijke tube, one can put:

$$\tilde{p} = \frac{p'}{p_0}\,, \quad \tilde{t} = \omega_0 t\,, \quad \tilde{u} = \frac{u'}{(a_0)_{\min}}\,, \quad \tilde{x} = \frac{x}{L}\,, \quad \tilde{T}_0 = \frac{T_0}{(T_0)_{\min}}\,, \quad \tilde{q} = \frac{q'_\vartheta L}{p_0 (a_0)_{\min}}\,, \quad \omega_0 = \frac{(a_0)_{\min}}{L}\,, \tag{1}$$

where tildes mark dimensionless quantities and ω_0 stands for the reference frequency. The latter is distinct from the primary fundamental oscillation mode, denoted by ω_1. The notation "min" refers to the tube's conditions that prevail at the upstream boundary, or inlet, where the temperature remains the lowest across the domain. The fundamental circular frequency for this system is defined as $\omega_1 = 2\pi f_1$, with f_1 representing the corresponding Hertzian frequency. These quantities can be further normalized to $\tilde{\omega}_1 = \omega_1/\omega_0$ and $\tilde{f}_1 = f_1/\omega_0$, respectively. Furthermore, the unsteady heat release, designated by q'_ϑ, may be made dimensionless using the problem's reference pressure, velocity, and lengthscale. Subsequently, through backward substitution of these non-dimensional quantities into the wave equation, and using $\varepsilon \equiv (\gamma - 1)/\gamma$ as a small perturbation parameter [20], one obtains:

$$\frac{\partial^2 \tilde{p}}{\partial \tilde{t}^2} - \tilde{T}_0 \frac{\partial^2 \tilde{p}}{\partial \tilde{x}^2} = \frac{\mathrm{d}\tilde{T}_0}{\mathrm{d}\tilde{x}} \frac{\partial \tilde{p}}{\partial \tilde{x}} + (\gamma - 1) \frac{\partial \tilde{q}}{\partial \tilde{t}} = \frac{\mathrm{d}\tilde{T}_0}{\mathrm{d}\tilde{x}} \frac{\partial \tilde{p}}{\partial \tilde{x}} + \varepsilon\gamma \frac{\partial \tilde{q}}{\partial \tilde{t}} \,. \tag{2}$$

The resulting expression incorporates the effects of both the temperature profile, $\tilde{T}_0(\tilde{x})$, and heat release rate, $\tilde{q}$.

B. Analytical Integral Approximation

To progress further in our analysis, the unsteady pressure field can be decomposed using $\tilde{p} = \tilde{p}^{(0)} + \varepsilon\tilde{p}^{(1)} + O(\varepsilon^2)$, where each superscript distinctly represents the perturbation order. It may be pertinent to note that knowledge of $\tilde{q}$ is not necessary at the leading order, when $\varepsilon \to 0$. As a first approximation, we are left with:

$$\frac{\partial^2 \tilde{p}^{(0)}}{\partial \tilde{t}^2} = \tilde{T}_0 \frac{\partial^2 \tilde{p}^{(0)}}{\partial \tilde{x}^2} + \frac{\mathrm{d}\tilde{T}_0}{\mathrm{d}\tilde{x}} \frac{\partial \tilde{p}^{(0)}}{\partial \tilde{x}} = \frac{\partial}{\partial \tilde{x}} \left(\tilde{T}_0 \frac{\partial \tilde{p}^{(0)}}{\partial \tilde{x}} \right) . \tag{3}$$

As shown by Polyanin [24], a comprehensive solution to Eq. (3) may be achieved using a Green's function formulation coupled with a Sturm–Liouville eigensolution. Before pursuing such a solution, however, it is convenient to specify a set of boundary conditions that are suitable for a Rijke tube. For this problem, we have:

$$\begin{aligned} \tilde{p}^{(0)} &= 0 \quad \text{at} \quad \tilde{x} = 0, \\ \tilde{p}^{(0)} &= 0 \quad \text{at} \quad \tilde{x} = 1, \\ \tilde{p}^{(0)} &= f_p(\tilde{x}) \quad \text{at} \quad \tilde{t} = 0, \\ \frac{\partial \tilde{p}^{(0)}}{\partial \tilde{t}} &= g_p(\tilde{x}) \quad \text{at} \quad \tilde{t} = 0. \end{aligned} \tag{4}$$

In the above, f_p and g_p represent the initial spatial configuration of the pressure wave throughout the tube along with its time-derivative, respectively. Then, having specified the governing equation and its auxiliary conditions, it may be helpful to revisit the integral solution to Eq. (3) as presented by Shelton and Majdalani [20]. One has

$$\tilde{p}^{(0)} = \frac{\partial}{\partial \tilde{t}} \left(\int_0^1 f_p(\xi) G_p\,(\tilde{x}, \xi, \tilde{t})\, \mathrm{d}\xi \right) + \int_0^1 g_p(\xi) G_p\,(\tilde{x}, \xi, \tilde{t})\, \mathrm{d}\xi, \tag{5}$$

where

$$G_p(\tilde{x}, \xi, \tilde{t}) = \sum_{n=1}^{\infty} \frac{y_n(\tilde{x}) y_n(\xi)}{\|y_n\|^2} \frac{\sin\left(\tilde{\omega}_n \tilde{t}\right)}{\tilde{\omega}_n}; \quad \|y_n\|^2 = \int_0^1 y_n^2(\tilde{x})\, \mathrm{d}\tilde{x}. \tag{6}$$

In Eqs. (5) and (6), ξ denotes the arbitrary source point integral associated with the Green's function formulation. Physically, it describes the interaction between two distinct spatial points: a source and a reference location. Moreover, G_p represents the Green's function for the pressure wave, which encapsulates both $\tilde{\omega}_n$ and $y_n(\tilde{x})$. These correspond to the eigenvalue and eigenfunction of the underpinning Sturm–Liouville equation, namely,

$$\frac{\mathrm{d}}{\mathrm{d}\tilde{x}} \left[\tilde{T}_0(\tilde{x}) \frac{\mathrm{d}y_n(\tilde{x})}{\mathrm{d}\tilde{x}} \right] + \tilde{\omega}_n^2 y_n(\tilde{x}) = 0; \qquad y_n(0) = y_n(1) = 0. \tag{7}$$

The homogeneous problem that we obtain can be solved either asymptotically, using approximation theory, or computationally, using a numerical eigensolver. For example, assuming sufficiently large eigenvalues, Eq. (7) can be approximated and expressed in a closed form using [20]:

$$\frac{y_n(\tilde{x})}{\|y_n\|} \approx \left[\frac{4}{\tilde{T}_0(\tilde{x}) \Theta^2} \right]^{1/4} \sin\left[\frac{\pi n}{\Theta} \int_0^{\tilde{x}} \frac{1}{\sqrt{\tilde{T}_0(\tilde{x})}}\, \mathrm{d}\tilde{x} \right]; \quad \Theta \equiv \int_0^1 \frac{1}{\sqrt{\tilde{T}_0(\tilde{x})}}\, \mathrm{d}\tilde{x}; \quad \tilde{\omega}_n \approx \frac{n\pi}{\Theta} \,. \tag{8}$$

By merging these asymptotic expressions with the Green's function formulation, a complete leading-order solution for the pressure waveform is therefore at hand. For example, using the Leibniz rule [25], the integration terms in Eq. (5) can be combined for a steady initial pressure distribution. One obtains:

$$\tilde{p}^{(0)} = \sum_{n=1}^{\infty} \frac{y_n(\tilde{x})}{\|y_n\|} \left[\cos(\tilde{\omega}_n \tilde{t}) \int_0^1 \frac{y_n(\xi)}{\|y_n\|} f_p(\xi)\, \mathrm{d}\xi + \frac{1}{\tilde{\omega}_n} \sin(\tilde{\omega}_n \tilde{t}) \int_0^1 \frac{y_n(\xi)}{\|y_n\|} g_p(\xi)\, \mathrm{d}\xi \right] . \tag{9}$$

The resulting solution is quite versatile because it can accommodate an arbitrary temperature distribution $\tilde{T}_0(\tilde{x})$ across the entire domain defined by $0 \leq \tilde{x} \leq 1$. Naturally, one assumes that the pressure at the domain's endpoint boundaries is accurately prescribed and that the temperature gradient remains smooth. These conditions allow for the precise prediction of the acoustic pressure modal shapes, frequencies, and propagation speeds directly from the mean temperature distribution, as long as the temperature gradient does not become excessively large. Nonetheless, these assumptions can be shown to deteriorate in the presence of a discontinuous or near-discontinuous temperature profile. Regardless of circumstances, however, the eigenfunctions can be accurately computed using a spectral collocation method, as thoroughly detailed by Trefethen [26]. In fact, we have verified the effectiveness of a spectral approach using 500 collocation points and an open-source Sturm-Liouville eigensolver that is well documented by Ledoux and Van Daele [21]. In view of the one-dimensional setting associated with a Rijke tube, only a brief computation time is required to achieve full convergence even in the case of an extensive number of collocation points.

Unlike the eigenfunctions, which may require the use of a numerical eigensolver in the event of steep thermal gradients, the frequency predictions achieved through Eq. (8) remain quite accurate [20]. In practice, closed-form expressions for the frequency can be produced so long as the integral of $[\tilde{T}_0(\tilde{x})]^{-1/2}$ in Eq. (8) can be analytically evaluated. Otherwise, a numerical solution may be readily pursued. In what follows, Eq. (9) will be validated using a sigmoidal thermal pattern that appears to be perfectly well-suited to model the Rijke tube's temperature distribution.

III. Acoustic Pressure Eigensolution

In this section, the effect of a thermally fluctuating flame zone or heat source of finite length will be examined. The dimensionless position of the heat source relative to the upstream edge of the tube will be specified as $\tilde{x}_f = x_f/L$, while its finite length, normalized by L, will be prescribed by $\tilde{l}_c = l_c/L$. In the same vein, assuming unit temperature upstream of the heat source, the normalized temperature downstream of the heat source will be designated as $\alpha = (T_0)_{\max}/(T_0)_{\min}$.

Former investigations that rely on the Green's function, such as those conducted by Bigongiari and Heckl [7], typically model the flame as being infinitesimally thin, thereby obviating the need to define the temperature profile within a flame zone of finite thickness. In reality, however, the temperature across the heat source remains gradual, and does not jump abruptly. Although it may exhibit a sharp rise, its increase may be characterized as being smooth and continuous. The present semi-analytical approach enables us to effectively capture this behavior, namely, of incorporating a realistic flame zone representing a heat source of finite length. This analysis is particularly valuable for assessing how variations in the temperature distribution's curvature within the flame zone can impact the acoustic pressure modes and their corresponding frequencies. Alternative studies, such as those by Heckl et al. [27] and Li and Morgans [8], explore varying thermal patterns, suggesting that the temperature variation could be locally approximated by either a constant-constant or piecewise linear fit to a variable profile. At present, the temperature profile will be permitted to gradually change across the flame zone, thereby mitigating the potential for abrupt thermal discontinuities.

Procedurally, a global temperature profile of the logistic or sigmoidal type will be adopted. This global profile has the advantage of remaining uniformly valid while spanning the entire length of the tube, including the flame zone, in a continuous and differentiable manner, thus precluding the need for piecewise thermal representations. The implementation of a global profile will primarily focus on the role of the temperature gradient in conjunction with an S-shaped sigmoidal function, which will be prescribed in Eq. (10) below. This particular sigmoidal function is adaptable and optimally configured to encapsulate the heat source region, especially where abrupt changes in the temperature occur, while still asymptoting to constant temperatures, $(T_0)_{\min}$ and $(T_0)_{\max}$, upstream and downstream of the flame zone. In the interest of clarity, visual illustrations of this global temperature distribution are provided in Fig. 2 using different sets of profile-defining parameters. These include user-specified values of $\tilde{x}_f = 0.25$, $\tilde{l}_c = \{0.1, 0.2, 0.3, 0.4\}$, $\alpha = 5$, and the corresponding sigmoidal growth rate or curve steepness β that may be analytically determined from Eq. (11).

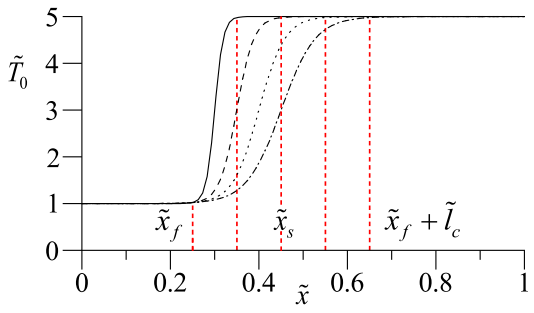

Fig. 2. Sigmoidal temperature distribution applied globally along a Rijke tube, as per Eq. (10), with $\tilde{l}_c = 0.1$ (solid), 0.2 (dashed), 0.3 (dotted), and 0.4 (dash-dotted). As per Eq. (11), steepness values consist of $\beta = 103.6$, 51.8, 34.5, and 25.9. We set the thermal gain at $\alpha = (T_0)_{\max}/(T_0)_{\min} = 5$ and the initial flame zone at $\tilde{x}_f = 0.25$.

A. Global Sigmoidal Temperature Profile

At this stage, we shift our focus to the S-shaped sigmoidal function. Unlike the piecewise approaches previously considered in other studies, this model provides a seamless, continuous, and differentiable temperature profile throughout the entire domain. Moreover, it enables us to capture the rapid temperature transition that occurs across the flame zone. The defining expression for the sigmoidal function may be written as

$$\tilde{T}_0(\tilde{x}) = \frac{A}{1 + e^{-\beta(\tilde{x} - \tilde{x}_s)}} + B; \tag{10}$$

where

$$A = \frac{\left(e^{\beta\tilde{x}_s} + 1\right)\left(e^{\beta\tilde{x}_s} + e^{\beta}\right)(\alpha - 1)\, e^{-\beta\tilde{x}_s}}{e^{\beta} - 1} \quad \text{with} \quad \tilde{x}_s = \tilde{x}_f + \tfrac{1}{2}\tilde{l}_c \quad \text{and} \quad B = 1 - \frac{A}{1 + e^{\beta\tilde{x}_s}}.$$

In this context, β denotes the rate of sigmoidal growth or steepness, which modulates the length of the narrow region (i.e, the "run") over which the most significant, and potentially abrupt, rise in temperature can occur. According to Fig. 2, one can observe that elevated β values result in sharper S-curves, thereby shortening the transitional "run" between the minimum and maximum temperatures, $(T_0)_{\min}$ and $(T_0)_{\max}$. This variation is depicted through curves using $\tilde{l}_c = 0.1$ (solid), 0.2 (dashed), 0.3 (dotted), and 0.4 (dash-dotted). The "rise" of the temperature, in this framework, is precisely defined by the parameter α. The term $\tilde{x}_s$ refers to the sigmoidal "midpoint" or "midrange," aligning with the axial position where the S-shaped curve intersects its median temperature value. To effectively simulate the flame zone segment within a Rijke tube, $\tilde{x}_s$ is ideally positioned at the center of the heat source element. For the cases depicted in Fig. 2, the parameters $\alpha = 5$ and $\tilde{x}_f = 0.25$ are consistently held constant. As for the β values, they are adjusted for each "run," $\tilde{l}_c$, to achieve the desired temperature rise α.

Conveniently, the steepness of the sigmoidal profile can be modified in a manner to permit the total temperature increase of the profile, denoted by α, to be precisely confined within a user-defined segment of length $\tilde{l}_c$. For example, by allowing the profile to extend from $\tilde{T}_0(\tilde{x}) = 1.01$ to $\tilde{T}_0(\tilde{x}) = 0.99\alpha$ over a specified combustor length, $\tilde{l}_c$, one can deduce the steepness parameter β that must be prescribed to achieve these predetermined specifications. Using a closed-form expression for the length of the combustor, one can further substitute the fast-converging large-β approximations, $A \approx \alpha - 1$ and $B \approx 1$, to obtain

$$\beta = \frac{1}{\tilde{l}_c} \ln\left[\frac{(A + B - 1.01)(B - 0.99\alpha)}{(B - 1.01)(A + B - 0.99\alpha)}\right] \approx \frac{1}{\tilde{l}_c}\left[\ln\left(0.99\alpha + 1.01\alpha^{-1} - 2\right) + 9.21\right]. \tag{11}$$

By way of example, in order to determine the sigmoidal growth rate for $\alpha = 4$ and $\tilde{l}_c = 0.1$, one finds an appropriate $\beta = 100.0$. For the conditions set in Fig. 2, where $\alpha = 5$, one finds $\beta = 103.6$ (solid), 51.8 (dashed), 34.5 (dotted), and 25.9 (dash-dotted) for $\tilde{l}_c = 0.1$, 0.2, 0.3, and 0.4, respectively. To further explore the behavior of this continuous global function, Eq. (10) is combined with Eqs. (8) and (9) to generate a series of acoustic pressure eigenvalues and eigensolutions using four specific variations in each of the main characteristic parameters. This is illustrated in Fig. 3 using $\alpha = \{2, 4, 6, 8\}$, $\tilde{x}_f = \{0, 0.25, 0.5, 0.75\}$, and $\tilde{l}_c = \{0.1, 0.2, 0.3, 0.4\}$ with either $\alpha = 4$ or 8. The analysis, which is supported by a spectral code with Chebyshev collocation points [26], is also validated against an open-source

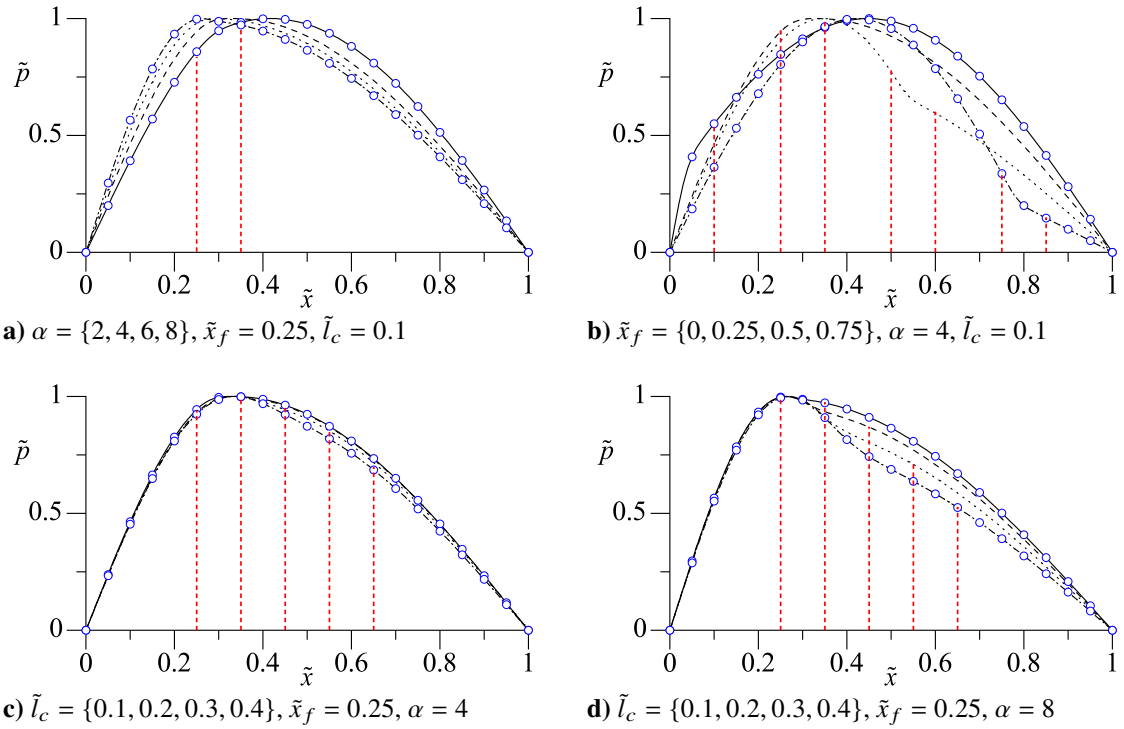

Fig. 3. Comparison of acoustic pressure mode shapes for four specific variations in a) α, b) $\tilde{x}_f$, and $\tilde{l}_c$ with either c) $\alpha = 4$ or d) 8 for the sigmoidal profile in Eq. (10). Individual variations defined in the subcaption of each part are denoted sequentially by solid, dashed, dotted, and dash-dotted lines. Hollow circles represent predictions obtained from an open-source solver developed by Ledoux and Van Daele [21]. Here, the sigmoidal steepness β values correspond to: a) {84.9, 100, 106, 110}, b) {85}, c) {100, 50.0, 33.3, 25.0}, and d) {110, 55.0, 36.7, 27.5}.

Strum-Liouville eigensolver[21], which is represented with hollow circles for each of the first and last cases considered in each part of Fig. 3. Clearly, both codes stand in perfect agreement.

The first general observation that may be gleaned from all parts of Fig. 3 is the absence of a discontinuity in any of the mode shapes. The curves are consistently smooth, continuous, and differentiable across the entire domain, specifically at both the upstream and downstream boundaries of the finite flame zone.

The second key insight pertains to the noticeable flattening of the pressure mode shapes past the flame's leading edge with successive increases in α, $\tilde{x}_f$, or $\tilde{l}_c$. This trend is clearly discernible from the illustrations in Figs. 3a–3c. The mode shapes exhibit an even more pronounced flattening in Fig. 3d, which can be substantially attributed to the thermal gain doubling from 4 in Fig. 3c to 8 in Fig. 3d. From a physical standpoint, as the length of the flame zone is elongated, β must decrease, leading to a more linear appearance in the corresponding mode shapes.

It is noteworthy that in the majority of cases analyzed, the heat source is maintained at $\tilde{x}_f = 0.25$. The third observation for these specific instances is the continuous leftward shift of the peak pressure antinodes, which progresses until the peaks become aligned with the quarter-length position of the flame zone. This shifting accompanies the flattening process and occurs with gradual increases in either α or $\tilde{l}_c$. Concurrently, this leftward shift of the peak pressure amplitudes contributes to a progressive straightening of the mode shape curvatures upstream of the flame zone, eventually rendering them into straight lines connecting the forward pressure node with the point of maximum amplitude.

The fourth observation concerns the mode shape behavior in Fig. 3b, where the heat source is relocated to $\tilde{x}_f = \{0, 0.25, 0.5, 0.75\}$, while keeping $\alpha = 4$ and $\tilde{l}_c = 0.1$. In strict conformance with acoustic theory and the global approximation examined so far, all positions in Fig. 3b, except for the quarter length station, reveal a sinusoidal mode shape pattern that is skewed in the vicinity of the flame zone boundaries.

Lastly, we note that, in both Figs. 3a and 3d, particularly when $\alpha \geq 4$, the peak pressure amplitude becomes more distinguishable due to the faster rate of pressure depreciation beyond its location.

In reflecting back on the present analysis, one may infer that the functional form that is selected to model the flame zone has a strong bearing on the resultant mode shape structures and their extremities, particularly at elevated thermal gains. Clearly, the adoption of a realistic thermal profile along a Rijke tube can be an essential prequel to undertaking a thorough thermoacoustic evaluation. Furthermore, the analysis seems to indicate that the length of the flame zone has a negligible impact on the position of the peak pressure amplitude, thereby supporting the thin sheet approximation that is often used in related investigations, such as those by Bigongiari and Heckl [7] and Li and Zhao [12].

IV. Acoustic Eigenmode Analysis

This section explores the connection between the modal frequency and the characteristic flame zone parameters. The analysis begins by closely examining the sigmoidal distribution that is prescribed by α, $\tilde{l}_c$, $\tilde{x}_f$, and β. The effect of increasing the mode number n is also investigated. Based on the frequency formulation given by Eq. (8), one can put

$$\tilde{\omega}_n = \frac{n\pi}{\Theta} \qquad \text{and so} \qquad \tilde{\omega}_1 = \frac{\pi}{\Theta} \qquad \text{where} \qquad \Theta = \int_0^1 \tilde{T}_0^{-1/2}\, \mathrm{d}\tilde{x}. \tag{12}$$

Naturally, the analysis will materially benefit from evaluating the eigenmodes associated with the global thermal distribution in closed form. After some effort, it may be shown that such an outcome is possible using both exact and asymptotic expansion techniques. Evidently, developing an analytical expression for the frequency will be quite advantageous as it will allow for direct predictions of its sensitivity to changes in flame zone parameters, including the location, length, temperature gain, sigmoidal growth rate, and thermal curvature.

A. Closed-Form Analytical Eigenfrequency

Substituting the sigmoidal profile given in Eq. (10) into Eq. (12), using "sig" for "sigmoidal," and recalling that $A \approx \alpha - 1$ and $B \approx 1$, a highly accurate and practical approximation for Eq. (12) may be produced. After some algebra, one finds

$$\Theta_{\text{sig}} \approx \frac{1}{\sqrt{\alpha}\beta} \ln\left\{ \frac{\left(\sqrt{\alpha} - \xi_1\right)\left(\sqrt{\alpha} + \xi_2\right)\left[\frac{(\xi_1+1)(\xi_2-1)}{(\xi_1-1)(\xi_2+1)}\right]^{\sqrt{\alpha}}}{\left(\sqrt{\alpha} + \xi_1\right)\left(\sqrt{\alpha} - \xi_2\right)} \right\}, \quad \xi_1 = \sqrt{\frac{e^{\beta\tilde{x}_s} + \alpha}{1 + e^{\beta\tilde{x}_s}}} \quad \text{and} \quad \xi_2 = \sqrt{\frac{e^{\beta\tilde{x}_s} + \alpha e^{\beta}}{e^{\beta} + e^{\beta\tilde{x}_s}}}. \tag{13}$$

Although Eq. (13) is compact, its precision proves rather limited to thermal gains not surpassing $\alpha = 8$. An exact formulation that remains uniformly applicable over all possible values of α may be obtained, albeit inherently more laborious. Its main drawback may be caused by its tendency to exhibit occasional singularities when $\tilde{x}_f > 0.65$ and $\tilde{l}_c < 0.1$. Its complete expression, which is suitable for the majority of practical configurations, can be written as:

$$\Theta_{\text{sig}} = \frac{2\sqrt{e^{\beta} - 1}}{\zeta_1 \beta} \left\{ i \left[\arccos\left(\frac{\zeta_1}{\sqrt{\left(e^{\beta} + e^{\beta\tilde{x}_s}\right)(\alpha - 1)}} \right) - \arccos\left(\frac{\zeta_1}{\sqrt{e^{\beta\tilde{x}_s}(\alpha - 1) + \alpha - 1}} \right) \right] \right.$$
$$\left. + \frac{\zeta_1 e^{\beta\frac{\tilde{x}_s}{2}}}{\sqrt{e^{\beta}(\alpha - 1) + e^{\beta\tilde{x}_s}\left(\alpha - e^{\beta}\right)}} \left[\operatorname{arccot}\left(\frac{e^{\beta\frac{\tilde{x}_s}{2}}\sqrt{e^{\beta} - 1}}{\zeta_2} \right) - \arctan\left(\frac{\zeta_2 e^{\beta\frac{\tilde{x}_s}{2}}}{\sqrt{\alpha\left(e^{\beta} - 1\right)}} \right) \right] \right\}, \tag{14}$$

where

$$\zeta_1 = \sqrt{e^{\beta\tilde{x}_s}(\alpha - 1) + e^{\beta}\alpha - 1} \quad \text{and} \quad \zeta_2 = \sqrt{e^{\beta}(\alpha - 1) + e^{\beta\tilde{x}_s}\left(\alpha - e^{\beta}\right)}. \tag{15}$$

As per Eq. (12), the acoustic frequency, for any mode number, can be conveniently retrieved using $\tilde{\omega}_{\text{sig}} = n\pi/\Theta_{\text{sig}}$.

B. Frequency Sensitivity to Thermal Properties

Based on the sigmoidal thermal distribution, the sensitivity of the fundamental frequency to the problem's characteristic parameters, α, $\tilde{x}_f$, $\tilde{l}_c$, and β, can be systematically investigated and summarized over a wide range of operating conditions. These consist of $1 \le \alpha \le 10$, $0 \le \tilde{x}_f \le 0.6$, $0.1 \le \tilde{l}_c \le 0.75$, and $10 \le \beta \le 110$. As shown

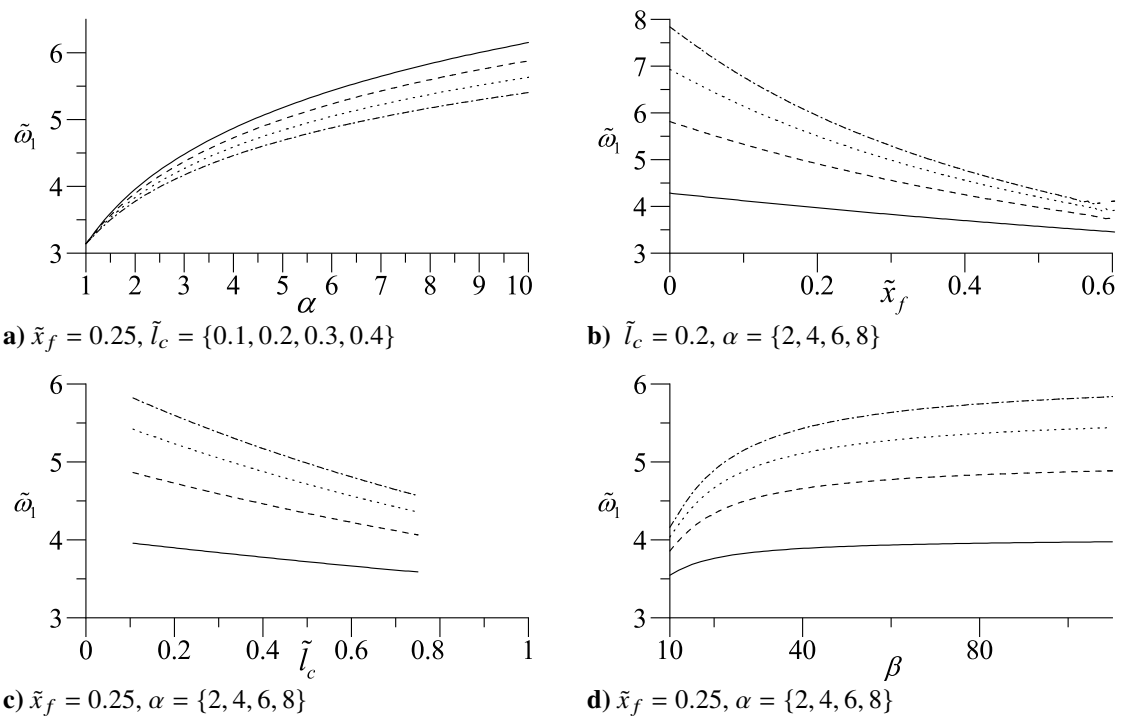

a) $\tilde{x}_f = 0.25$, $\tilde{l}_c = \{0.1, 0.2, 0.3, 0.4\}$ **b)** $\tilde{l}_c = 0.2$, $\alpha = \{2, 4, 6, 8\}$

c) $\tilde{x}_f = 0.25$, $\alpha = \{2, 4, 6, 8\}$ **d)** $\tilde{x}_f = 0.25$, $\alpha = \{2, 4, 6, 8\}$

Fig. 4. Frequency variations with a) α at fixed values of $\tilde{l}_c = \{0.1, 0.2, 0.3, 0.4\}$, followed by b) $\tilde{x}_f$, c) $\tilde{l}_c$, and d) β at fixed values of $\alpha = \{2, 4, 6, 8\}$ using the sigmoidal profile. These are denoted, successively, by solid, dashed, dotted, and dash-dotted lines.

in Fig. 4, these are varied one at a time while holding the other parameters at their benchmark values of $\tilde{x}_f = 0.25$, $\tilde{l}_c = 0.2$, and $\alpha = \{2, 4, 6, 8\}$. These ranges are selected in a manner to cover a broad practical range of operating parameters without driving the sigmoidal steepness β to excessive levels. As usual, any specific β value can be computed for an arbitrary combination of $\tilde{l}_c$ and α using Eq. (11).

Starting with the quarter length position benchmark, $\tilde{x}_f = 0.25$, it may be seen in Fig. 4a that $\tilde{\omega}_1$ undergoes a rapid increase that becomes gradually less prominent as the thermal gain is elevated from $\alpha = 1$ to 10. The frequency also diminishes as the flame zone thickness is increased and, in turn, the sigmoidal steepness β is reduced. Specifically at $\alpha = 10$, the frequency diminishes by 0.98 when the flame zone's length is quadrupled. This behavior is further confirmed in Fig. 4c where one can observe that widening the flame zone while maintaining a constant thermal gain leads to a lower frequency. Along similar lines, Figs. 4b–4d demonstrate that larger thermal gains produce higher frequencies when the remaining parameters are held constant. For example, quadrupling the thermal gain in Fig. 4b while maintaining $\tilde{l}_c = 0.2$ and $\tilde{x}_f = 0.25$ results in a sizable frequency increase of 1.7. Then, in both Figs. 4b and 4c, the fundamental frequency, $\tilde{\omega}_1$, decreases monotonically as the initial axial position, $\tilde{x}_f$, is moved downstream or as the length of the flame zone, $\tilde{l}_c$, is gradually incremented. These changes result in the temperature rise occurring further downstream, thus reducing the effective heated length of the tube closer to the inlet. Interestingly, the relation between the frequency and both $\tilde{x}_f$ and $\tilde{l}_c$ approaches a nearly linear trend as the thermal gain is reduced to a moderate value of $\alpha = 2$. This linearity becomes even more prominent in the practical range of $1 \leq \alpha < 2$.

Lastly, we find in Fig. 4d that elevating β, which quickens the temperature rise around $\tilde{x}_f + \tilde{l}_c/2$, will cause the frequency to increase. This upward shift with β becomes even more pronounced for higher thermal gains. For example, quadrupling the latter at $\beta = 100$ leads to a frequency jump of 1.84.

In summary, the present analysis suggests that successive increases in the acoustic frequency can be systematically achieved by (i) elevating the temperature gain across the heat source, (ii) retracting the flame zone location to the tube's inlet, (iii) shortening the flame zone segment, and (iv) reducing the steepness of the thermal profile at the downstream edge of the flame zone. These findings provide valuable considerations for the design and optimization of thermoacoustic systems. Furthermore, given that $\tilde{\omega}_n = n\tilde{\omega}_1$ in Eq. (12), the same trends will apply identically to all harmonic modes.

V. Conclusion

In this work, we revisit the thermoacoustic characteristics of a one-dimensional tube that incorporates a heat source whose position, length, temperature gain, and local thermal gradient can be adjusted. Using an asymptotic approximation for the oscillatory pressure field in a one-dimensional enclosure, we manage to derive the corresponding eigenvalues and eigensolutions through an integral formulation that is paired with a spectral collocation eigensolver. Since the analytical framework is intrinsically linked to the temperature distribution, a uniformly valid thermal profile exhibiting a sigmoidal character is implemented globally across the entire length of the tube, including the flame zone.

Most studies that model the heat source element in a Rijke tube assume an infinitely thin flame zone that is bracketed by two thermal profiles using a piecewise formulation. At the outset, a temperature jump is frequently realized across the flame zone. In the present framework, we avoid the discontinuities attributed to sudden jumps through reliance on a sigmoidal function to describe the temperature variation uniformly across the enclosure. The resulting approach offers multiple distinct advantages that may be worth enumerating. These include: (i) the smoothing of pressure mode shapes across flame zone edges where piecewise approximations lead to sharp kinks; (ii) the ability to accommodate both gradual and rapid temperature changes within the flame zone; (iii) the ability to specify a sigmoidal midpoint that aligns with the center of the flame zone; (iv) the ability to specify a sigmoidal growth rate or steepness β that controls the effective length of the flame zone; (v) the ability to tailor the sigmoidal distribution to emulate a user-defined temperature distribution over a finite segment; and (vi) the ability to predict the acoustic waveforms and frequencies strictly analytically. As such, a globally applied thermal field enables us to enhance our physical understanding of the observed thermoacoustic phenomena and their relations to key system parameters.

Moreover, our analysis reveals that the temperature gain α has the most appreciable effect on the pressure mode shapes. For instance, with the flame zone located at $\tilde{x}_f = 0.25$ and for $\alpha = 1$, doubling the latter shifts the peak pressure amplitude from the tube's midpoint to the quarter length position; any further increases in α result in progressively flatter mode shapes. The length of the flame zone, $\tilde{l}_c$, is also found to impact the mode shapes similarly to α. Displacing the flame zone location, $\tilde{x}_f$, rearward causes the pressure antinode to shift towards the tube's midpoint, particularly as the tube approaches an isothermal state. Along similar lines, variations in $\tilde{l}_c$ affect the mode shape structure, with reductions producing curved mode shapes and elongations leading to spatially linear pressure variations.

Finally, given the ability to determine the acoustic frequencies for a global thermal pattern using an analytical expression, our analysis shows that higher frequencies can be achieved by (a) elevating the temperature gain across the heat source, (b) positioning the flame zone closer to the tube's leading edge, (c) shortening the flame zone segment, and (d) reducing the thermal profile's steepness near the downstream boundary. We conclude by highlighting the effectiveness of the resulting framework at overcoming the issues of discontinuous temperature jumps as well as the pitfalls of dismissing the flame zone thickness. We also note that a proper choice of a thermal profile can have a substantial bearing on the overall pressure mode shapes and frequencies, particularly for large thermal gains and extensive heat source lengths. In future analysis, we aim to expand the present framework to include velocity modes.

Acknowledgements

This work was supported partly by the National Science Foundation, through grant № CMMI-1761675, and partly by the Hugh and Loeda Francis Chair of Excellence, Department of Aerospace Engineering, Auburn University. None of this work would have been remotely possible were it not for the technical guidance provided by Cody M. Shelton.

References

[1] Carrier, G. F., "The Mechanics of Rijke Tube," *Quarterly of Applied Mathematics*, Vol. 12, No. 4, 1955, pp. 383–395. doi:10.1090/qam/69698.

[2] Chu, B.-T., "Stability of Systems Containing a Heat Source - The Rayleigh Criterion," Research Memorandum 56D27, 1956.

[3] Miller, J. and Carvalho, J. A., "Comments on Rijke Tube," *Scientific American*, Vol. 204, No. 3, 1961, pp. 180–182.

[4] Maling, G. C., "Simplified Analysis of the Rijke Phenomenon," *Journal of the Acoustical Society of America*, Vol. 35, 1963, pp. 1058–1060. doi:10.1121/1.1918658.

[5] Zinn, B. T., "State of the Art and Research Needs of Pulsating Combustion," *Noise Control and Acoustics*, Vol. 18 of *Winter Annual Meeting*, American Society of Mechanical Engineers, ASME, New Orleans, LA, 1984, pp. 1–7.

[6] Raun, R. L., Beckstead, M. W., Finlinson, J. C., and Brooks, K. P., "Review of Rijke Tubes, Rijke Burners and Related Devices," *Progress in Energy and Combustion Science*, Vol. 19, No. 4, 1993, pp. 313–364. doi:10.1016/0360-1285(93)90007-2.

[7] Bigongiari, A. and Heckl, M. A., "A Green's Function Approach to the Rapid Prediction of Thermoacoustic Instabilities in Combustors," *Journal of Fluid Mechanics*, Vol. 798, 2016, pp. 970–996. doi:10.1017/jfm.2016.332.

[8] Li, J. and Morgans, A. S., "The One-Dimensional Acoustic Field in a Duct with Arbitrary Mean Axial Temperature Gradient and Mean Flow," *Journal of Sound and Vibration*, Vol. 400, 2017, pp. 248–269. doi:10.1016/j.jsv.2017.03.047.

[9] Lieuwen, T. C., *Unsteady Combustor Physics*, Cambridge University Press, 2012.

[10] Veeraragavan, A., Pesala, B., and Sujith, R., "An Integral Approach to Modeling Sound Propagation through a Finite Combustion Zone," *44th AIAA Aerospace Sciences Meeting and Exhibit, AIAA Paper 2006-0542*, American Institute of Aeronautics and Astronautics, Jan. 2006. doi:10.2514/6.2006-542.

[11] Matveev, K. I. and Culick, F. E. C., "A Study of the Transition to Instability in a Rijke Tube with Axial Temperature Gradient," *Journal of Sound and Vibration*, Vol. 264, No. 3, 2003, pp. 689–706. doi:10.1016/s0022-460x(02)01217-8.

[12] Li, X. and Zhao, D., "Mean Temperature Effect on a Thermoacoustic System Stability and Non-Normality," *Journal of Low Frequency Noise, Vibration and Active Control*, Vol. 34, No. 2, June 2015, pp. 185–200. doi:10.1260/0263-0923.34.2.185.

[13] Poinsot, T., "Prediction and Control of Combustion Instabilities in Real Engines," *Proceedings of the Combustion Institute*, Vol. 36, No. 1, 2017, pp. 1–28. doi:10.1016/j.proci.2016.05.007.

[14] McManus, K., Poinsot, T., and Candel, S., "A Review of Active Control of Combustion Instabilities," *Progress in Energy and Combustion Science*, Vol. 19, No. 1, Jan. 1993, pp. 1–29. doi:10.1016/0360-1285(93)90020-f.

[15] O'Connor, J., Acharya, V., and Lieuwen, T., "Transverse Combustion Instabilities: Acoustic, Fluid Mechanic, and Flame Processes," *Progress in Energy and Combustion Science*, Vol. 49, August 2015, pp. 1–39. doi:10.1016/j.pecs.2015.01.001.

[16] Chen, T. Y., Hegde, U. G., Daniel, B. R., and Zinn, B. T., "Flame Radiation and Acoustic Intensity Measurements in Acoustically Excited Diffusion Flames," *Journal of Propulsion and Power*, Vol. 9, No. 2, 1993, pp. 210–216. doi:10.2514/3.23611.

[17] Lieuwen, T., "Modeling Premixed Combustion-Acoustic Wave Interactions: A Review," *Journal of Propulsion and Power*, Vol. 19, No. 5, 2003, pp. 765–781. doi:10.2514/2.6193.

[18] Flandro, G. A., Fischbach, S. R., and Majdalani, J., "Nonlinear Rocket Motor Stability Prediction: Limit Amplitude, Triggering, and Mean Pressure Shift," *Physics of Fluids*, Vol. 19, No. 9, 2007, pp. 094101–16. doi:10.1063/1.2746042.

[19] Culick, F. E. C., "Nonlinear Behavior of Acoustic Waves in Combustion Chambers—I," *Acta Astronautica*, Vol. 3, No. 9-10, September 1976, pp. 715–734. doi:10.1016/0094-5765(76)90107-7.

[20] Shelton, C. M. and Majdalani, J., "Different Perspectives on Predicting the Thermoacoustic Energy Conversion Response in a Rijke Tube," *Physics of Fluids*, Vol. 33, No. 11, November 2021, pp. 114110–30. doi:10.1063/5.0072193.

[21] Ledoux, V. and Van Daele, M., "Matslise 2.0: A Matlab Toolbox for Sturm–Liouville Computations," *ACM Transactions on Mathematical Software*, Vol. 42, No. 4, 2016, pp. 1–18. doi:10.1145/2839299.

[22] Kovàsznay, L. S. G., "Turbulence in Supersonic Flow," *Journal of the Aeronautical Sciences*, Vol. 20, No. 10, October 1953, pp. 657–674. doi:10.2514/8.2793.

[23] Morse, P. M. and Ingard, K. U., *Theoretical Acoustics*, Princeton University Press, January 1987.

[24] Polyanin, A. D., *Handbook of Linear Partial Differential Equations for Engineers and Scientists*, Chapman and Hall/ CRC, 2002.

[25] Stewart, J., Clegg, D. K., and Watson, S., *Calculus*, Cengage Learning, 9th ed., April 2020.

[26] Trefethen, L. N., *Spectral Methods in MATLAB*, Vol. 10, Society for Industrial and Applied Mathematics, January 2000. doi:10.1137/1.9780898719598.

[27] Heckl, M. A., Gopinathan, S. M., and Surendran, A., "A Unified Framework for Acoustic Instabilities Based on the Tailored Green's Function," *Journal of Sound and Vibration*, Vol. 541, December 2022, pp. 117279. doi:10.1016/j.jsv.2022.117279.